Crystal and magnetic structure of $Eu_4Ga_8Ge_{16}$

M. Christensen,[1] J. D. Bryan,[2] H. Birkedal,[2] G. D. Stucky,[2] B. Lebech,[3] and B. B. Iversen[1,*]
[1]*Department of Chemistry, University of Aarhus, DK-8000 Aarhus C, Denmark*
[2]*Department of Chemistry, University of California, Santa Barbara, California 93106, USA*
[3]*Materials Research Department, Risø National Laboratory, DK-4000 Roskilde, Denmark*
(Received 3 April 2003; revised manuscript received 4 September 2003; published 25 November 2003)

The antiferromagnetic ordering and crystal structure of the clathrate compound $Eu_4Ga_8Ge_{16}$ was investigated using multitemperature neutron and synchrotron x-ray powder diffraction. High-resolution low-Q neutron data were measured at long wavelength ($\lambda = 4.2$ Å) between 1.5 and 15 K for an accurate description of the magnetic structure, whereas high-Q diffraction patterns were collected using neutrons of wavelength 1.9 Å at the same temperatures to determine the nuclear structure precisely. The structure orders antiferromagnetically at about 8 K with ferromagnetic chains parallel to the a axis. The intrachain Eu-Eu distance, 4.1216(1) Å at 1.5 K, is significantly shorter than the distance observed in the ferromagnetic clathrates β-$Eu_8Ga_{16}Ge_{30}$ (5.23 Å) and α-$Eu_8Ga_{16}Ge_{30}$ (5.56 Å). Antiferromagnetic coupling to the nearest and next-nearest chains at distances of 5.99 and 6.98 Å, respectively, leads to an overall antiferromagnetic structure. A fit to a power law of the temperature dependence of the ordered Eu^{2+} magnetic moment results in a moment of $7.01(7)\mu_B$ at 0 K in agreement with the $7\mu_B$ for the free ion value of Eu^{2+}. The temperature dependence of the crystal structure was investigated from 11 K to room temperature using synchrotron x-ray powder diffraction. Analysis of the atomic displacement parameters with Einstein and Debye models gives $\Theta_E = 82(3)$ K for the guest atom and $\Theta_D = 266(4)$ K for the framework atoms. Based on Θ_D the lattice contribution to thermal conductivity is estimated to be 0.0125 W/cm K.

DOI: 10.1103/PhysRevB.68.174428 PACS number(s): 75.50.Ee, 61.10.Nz, 61.12.Ld, 72.15.Eb

I. INTRODUCTION

In recent years clathrate structures have been intensely investigated due to their potential use as thermoelectric materials.[1–8] The inorganic clathrate structures consist of semiconducting frameworks with oversized voids occupied by guest atoms. They can be classified into different types depending on the framework geometry.[9] The most studied class of materials is the type-I structures containing 46 framework atoms and 8 guest atoms in the unit cell giving typical stoichiometries of $M_8A_8B_{38}$ and $M_8A_{16}B_{30}$ depending on the nature of the guest atom (M) and the framework dopant (A). Recently several groups have also focused on the type-II structures with stoichiometry $M_{24}B_{136}$, which contains a very large 28-atom cage that can therefore accommodate larger guest atoms such as caesium or rubidium.[10,11] A new type of clathrate, $Eu_4Ga_8Ge_{16}$ (Refs. 12 and 13) was discovered as a minority phase during synthesis of the magnetic type-I clathrate $Eu_8Ga_{16}Ge_{30}$.[14] So far, relatively few magnetic clathrates have been synthesized,[15,16] but there is potentially a large interest in such systems since they could provide excellent examples of magnetic semiconductors (Kondo insulators, heavy fermion systems). In Paper II we report the magnetic susceptibility, the spin-flop phase diagram, Mössbauer spectra, and heat capacity of $Eu_4Ga_8Ge_{16}$.[17] In the present paper, Paper I, we examine in detail both the magnetic and the crystal structure of $Eu_4Ga_8Ge_{16}$ based on multitemperature neutron and synchrotron x-ray powder-diffraction data.

II. EXPERIMENT

A. Neutron powder diffraction

The data were recorded on a powder sample of ^{153}Eu enriched $Eu_4Ga_8Ge_{16}$. The enriched sample was prepared by the flux growth technique[12] using 98.7% enriched ^{153}Eu (Oak Ridge National Laboratory).[18] The product contains a mixture of the $Eu_4Ga_8Ge_{16}$ phase and Ge (diamond structure), and separation of the two phases is difficult without loss of the costly enriched $Eu_4Ga_8Ge_{16}$ phase. However, there is only limited overlap between the $Eu_4Ga_8Ge_{16}$ and Ge phases in the diffraction pattern and the mixture could therefore be used ''as is.'' The total weight of the synthesis product containing both phases was about 300 mg.

The neutron-diffraction experiments were performed at the quasicontinuous neutron spallation source (SINQ) at the Paul Scherrer Institute (PSI) in Switzerland. A 4-mm cylindrical textured aluminum sample holder was used, which does not interfere with the low-Q region (Q is the scattering vector) of $Eu_4Ga_8Ge_{16}$ where the magnetic peaks are observable. Two different neutron powder diffractometers were used in order to obtain precise information about both the magnetic and the crystal structures. The low-Q data were collected using the DMC neutron powder diffractometer located at the cold neutron source at SINQ. A vertically focusing (002) graphite monochromator was used to select neutrons of wavelength 4.2 Å. The DMC instrument is equipped with a banana-shaped position sensitive detector covering a total of 80° with 400 channels at 0.2° intervals. Two diffraction patterns with extremely good statistics were measured at 1.5 and 15 K, i.e., below and above the magnetic-phase-transition temperature. These data sets were used to determine and refine the magnetic structure. In addition, a set of diffraction patterns with less precise statistics were collected at different temperatures between 1.5 and 30 K in order to monitor the temperature dependence of the magnetic order. The temperature was changed in small steps across the phase transition always stepping from low to high temperature in order to minimize possible magnetic hysteresic effects. In

addition to the low-Q diffraction data, high-Q data were recorded on the HRPT powder diffractometer at SINQ. This instrument is situated at the thermal neutron source and equipped with a large position sensitive detector containing 1600 channels at 0.1° intervals covering a total scattering angle span of 160°. The (511)-reflection from a vertically focusing Ge monochromator provided a wavelength of 1.884 Å. Diffraction patterns were measured at 1.5 and 15 K. The sample environment in both experiments was controlled by a helium cryostat (Orange ILL type), which was moved intact between the two instruments. The sample was never removed from the cryostat nor heated above 30 K during the experiment.

B. Crystal structure refinement

The crystal structure was refined against the high temperature data (15 K) from both DMC and HRPT using the Rietveld refinement program FULLPROF.[19] The starting model was taken from the single-crystal x-ray-diffraction study of Bryan *et al.*[12] For the HRPT data the aluminum peaks from the sample container were excluded from the fit. For the DMC data a single Ge peak was removed. The absorption correction and scale factor were found to heavily influence the atomic displacement parameters (ADP's). The sample absorption coefficient was measured at 1.884 Å ($\mu R = 0.226$), whereas the 4.194-Å value was obtained by multiplication of the wavelength ratio. In order to get a stable and physically meaningful refinement, the ADP's were fixed to the values obtained from synchrotron powder-diffraction data recorded at matching temperatures. From HRPT refinements the percentage mol fraction of Ge was found to be 24.0(4)%.

The $Eu_4Ga_8Ge_{16}$ system has a framework structure belonging to the orthorhombic space group *Cmcm*. Refinement of the nuclear diffraction pattern gave lattice parameters of $a = 4.1216(1)$ Å, $b = 11.2470(2)$ Å, and $c = 13.1945(2)$ Å at 15 K. The framework is built from Ga and Ge with three unique sites each having a multiplicity of 8. The distribution of Ge and Ga over the framework is difficult to determine by x-ray diffraction, because the scattering power differs by only one electron. The somewhat larger difference in the neutron-scattering lengths between Ga and Ge (7.29 and 8.19 fm, respectively) may allow determination of preferred sitting. However, the problems with the ADP's prevented conclusive determination of the exact framework siting. Chakoumakos *et al.* concluded based on single-crystal neutron-diffraction data on $Eu_8Ga_{16}Ge_{30}$ that the framework in that structure is fully disordered,[14] although accurate maximum entropy method analysis of single-crystal x-ray diffraction of $Ba_8Ga_{16}Ge_{30}$ and $Sr_8Ga_{16}Ge_{30}$ indicate a Ga preference for a specific site ($6c$ of space group number 223).[4] In the present refinements a model containing randomly distributed Ga and Ge atoms at each framework site was employed. In the refined model the Eu atoms are located in the centers of the framework voids at the $4c$ site in space group *Cmcm* ($y \approx 0.207$). The agreement factors for the different models are listed in Table I.

C. Synchrotron x-ray powder diffraction

High-resolution synchrotron powder-diffraction measurements were carried out at the beam line BL02B2 at SPring8, Japan. The large Debye-Scherrer camera with an image plate detector was used to record the data.[20] A small fraction of the enriched sample used for the neutron experiment was sealed in a 0.1-mm glass capillary. The capillary was mounted in a helium Displex refrigerator (1 K precision). The incident x-ray wavelength ($\lambda = 0.42061$ Å) was determined by calibration on a standard CeO_2 sample ($a = 5.411\,102$ Å). The image plates were scanned with a pixel resolution of 100 μm. Datasets were recorded from 11 to 300 K in steps of about 20 K. The exposure time was 10 min in all cases except for the 11-K data, where 90 min exposure time was used. All data sets extend from $2\theta = 3°$ to $2\theta = 75°$ with a step size of 0.01°. Rietveld refinements were performed using GSAS.[21] Besides the $Eu_4Ga_8Ge_{16}$ phase, the Ge impurity was also modeled. The background was described by an interpolation formula linear in 2θ. Due to the small diameter of the capillary and the high energy of the incoming x rays, absorption effects are negligible. The molar fraction of Ge refined to 31.8(1)%. The displex induces jumps in the background around 38.5° and 49.3°; the regions 37.98°–40.50° and 48.50°–50.00° were excluded from the fit. Figure 1 shows the agreement obtained at 11 K, but the quality of the fit is similar at all temperatures. The refined structural parameters are listed in Table II.

III. RESULTS AND DISCUSSION

A. Magnetic structure

The magnetic structure originates from the $4f$ electrons of the ionically bound Eu guest atoms. From Mössbauer data it is known that Eu is in the $+2$ oxidation state.[17] The $+2$ oxidation state of Eu is in accordance with the Zintl concept, where the electropositive guest atoms donate electrons to the framework. The DMC data measured above the phase-transition temperature were subtracted from the 1.5-K data to reveal the magnetic peaks (assuming that the crystal structure is unchanged). The diffraction patterns as well as the difference pattern are shown in Fig. 2. The first magnetic peak in the diffraction pattern would correspond to the (001) reflection of the crystal cell if allowed by symmetry. The absence of peaks below (001) suggests there is no magnetic superstructure, i.e., the magnetic unit cell coincides with the crystal. The antiferromagnetic structure was investigated using different models for the direction of the magnetic moments. For each model the magnetic structure factor was compared with the measured data. A model accounting for the intensities of the magnetic diffraction peaks have the moments of the four Eu atoms in the unit cell along the following directions: $m_1 = (U,V,W)$, $m_2 = (-U,-V,-W)$, $m_3 = (U,V,W)$, $m_4 = (-U,-V,-W)$, where U, V, and W are the magnetic moments along the a, b, and c axes, respectively. This model was used in the program FULLPROF to fit the magnetic moments.[20] The crystal structure was fixed at the values from the measurement above the phase transition. Free refinement of this model gave $U = 6.13(5)\mu_B$ and W

TABLE I. Crystallographic details for $Eu_4Ga_8Ge_{16}$ from neutron powder-diffraction experiments. A sixth-order polynomial background function was used. T = temperature, λ = wavelength, μR = absorption correction. The agreement factors are defined by $R_p=\Sigma|y_{o,i}-y_{c,i}|/\Sigma|y_{o,i}|$, $R_{wp}=[\Sigma w_i|y_{o,i}-y_{c,i}|^2/\Sigma w_i|y_{o,i}|^2]^{1/2}$, $\chi^2=\Sigma w_i|y_{o,i}-y_{c,i}|^2/\sigma_i^2$, $R_I=\Sigma|I_o-I_c|/\Sigma|I_o|$, $R_F=\Sigma|F_o-F_c|/\Sigma|F_o|$, R_{magnetic} is similar to R_F but for the magnetic peaks, μ_a is the magnetic moment along the a axis.

	Crystal structure		Moment along a and c axis		Moment along a axis	
Instrument	HRPT	DMC	HRPT	DMC	HRPT	DMC
T (K)	15.0	15.0	1.5	1.5	1.5	1.5
λ (Å)	1.884	4.194	1.884	4.194	1.884	4.194
μR	0.226	0.503	0.226	0.503	0.226	0.503
No. data points	2763	912	2763	912	2763	912
No. $Eu_4Ga_8Ge_{16}$ nuclear reflections	235	21	235	21	235	21
No. Ge nuclear reflections	11		11		11	
No. magnetic reflections ($I_{hkl}>1\%\cdot I_{001}$)			5	16	5	16
Background parameters	6	6	6	6	6	6
Nuclear profile parameters	12	4	2	1	2	1
Nuclear parameters	14	12				
Magnetic profile parameters			6	4	6	4
Magnetic parameters			4	4	3	3
Total no. of parameters	32	22	18	15	17	14
R_p (%)	6.13	6.64	6.71	9.80	6.73	10.3
R_{wp} (%)	8.23	8.43	8.69	12.3	8.71	12.8
χ^2	14.7	6.01	14.8	17.8	14.9	19.0
$R_I(Eu_4Ga_8Ge_{16})$ (%)	13.0	8.05	10.5	7.51	10.6	8.03
$R_F(Eu_4Ga_8Ge_{16})$ (%)	9.90	5.96	7.1	4.73	7.09	5.13
R_I(Ge) (%)	4.68		4.28		4.31	
R_F(Ge) (%)	2.17		2.41		2.43	
$R_{(\text{magnetic})}$ (%)			10.4	10.1	9.98	11.6
$\mu_a(\mu_B)$			6.13(5)		6.55(5)	
$\mu_c(\mu_B)$			1.77(18)			
$\mu_{\text{tot}}(\mu_B)$			6.38(6)		6.55(5)	

$=1.77(18)\mu_B$. No moment along b (V) was detected, and the refinement gave a total magnetic moment of $6.38(6)\mu_B$ at 1.5 K. The magnetic R factor is 10.1% for this model. Using the space group, the position of the europium atoms and the propagation vector as input to the program SARAH the possible directions of the magnetic moments were calculated.[22] Based on Landau theory for second-order phase transitions, the component should be along either the a, b, or c axis.[23] Taking these symmetry arguments into account, the magnetic moments along the b and c axis were forced to zero and only the moment along a was refined. This model gave a magnetic moment of $6.55(5)\mu_B$ at 1.5 K, but the magnetic R factor increased to 11.6%. This is higher than the model with the moment along both the a and c axes. Nevertheless, the a-axis model is supported by careful susceptibility measurements.[17] No improvement in the refinement was obtained by including aspherical terms in the scattering expression (decrease of the Landé g factor). It should be noted that the structural disorder of the Eu atoms is quite large along the c axis (see below). Disorder of the Eu atoms could potentially be modeled with a magnetic component along the c axis. The most convincing model based on the agreement with theory and susceptibility measurements places the magnetic moments solely parallel to the a axis. The crystal and magnetic structures are sketched in Fig. 3. The magnetic structure can be described as one-dimensional chains running parallel to the a axis. The magnetic moment of the atoms

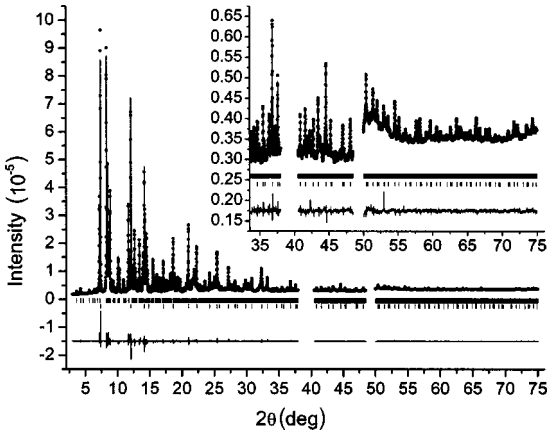

FIG. 1. Synchrotron x-ray powder diffraction at 15 K. Crosses are the data points, and the solid line the Rietveld model. The bottom shows the difference pattern.

TABLE II. Crystallographic details for $Eu_4Ga_8Ge_{16}$ from synchrotron powder-diffraction data. The definitions of the agreement factors are given in Table I. H1, H2, and H3 refer to the framework atoms (Ga/Ge).

T (K)	11	30	45	60	75	90	110	130
No. data points	6795	6795	6795	6795	6795	6795	6795	6795
No. reflections	4975	4996	4976	4980	4981	4982	4983	4987
No. parameters	66	66	66	66	66	66	66	66
R_p (%)	3.04	3.54	3.54	3.51	3.50	3.59	3.46	3.36
R_{wp} (%)	4.61	5.37	5.35	5.24	5.26	5.40	4.99	4.85
χ^2 (%)	38.09	5.91	5.81	5.74	5.72	5.83	5.29	5.42
R_I (%)	3.21	3.81	3.92	4.04	3.79	3.84	3.90	4.22
a	4.121 92(5)	4.122 14(5)	4.122 45(5)	4.122 87(5)	4.123 37(5)	4.124 01(6)	4.124 86(5)	4.125 96(5)
b	11.2470(1)	11.2475(2)	11.2483(2)	11.2491(2)	11.2503(2)	11.2520(2)	11.2541(2)	11.2568(2)
c	13.1954(2)	13.1965(2)	13.1973(2)	13.1981(2)	13.1996(2)	13.2013(2)	13.2039(2)	13.2068(2)
y(Eu)	0.206 96(7)	0.206 85(8)	0.206 89(8)	0.207 19(7)	0.207 06(7)	0.207 26(8)	0.207 08(7)	0.207 42(8)
U^{11}(Eu) (10^{-4} Å^2)	30(4)	31(4)	36(5)	29(4)	39(5)	50(5)	51(5)	59(5)
U^{22}(Eu) (10^{-4} Å^2)	65(4)	59(5)	65(5)	67(5)	65(5)	65(5)	78(5)	94(6)
U^{33}(Eu) (10^{-4} Å^2)	111(4)	115(5)	116(5)	137(5)	156(5)	157(6)	170(6)	167(6)
y(H1)	−0.070 23(9)	−0.0700(1)	−0.0700(1)	−0.0696(1)	−0.0696(1)	−0.0695(1)	−0.0700(1)	−0.0698(1)
z(H1)	0.343 64(8)	0.343 42(9)	0.343 46(9)	0.343 63(9)	0.343 62(9)	0.3436(1)	0.343 42(9)	0.343 59(9)
U(H1) (10^{-4} Å^2)	13(3)	24(3)	27(3)	22(3)	31(3)	30(3)	41(3)	50(3)
y(H2)	0.026 90(8)	0.0271(1)	0.0271(1)	0.0267(1)	0.0266(1)	0.0265(1)	0.026 55(9)	0.0264(1)
z(H2)	0.408 30(9)	0.4088(1)	0.4087(1)	0.4085(1)	0.4083(1)	0.4082(1)	0.4082(1)	0.4086(1)
U(H2) (10^{-4} Å^2)	21(3)	18(3)	17(3)	18(3)	23(3)	25(3)	32(3)	36(3)
y(H3)	0.243 99(9)	0.2439(1)	0.2439(1)	0.2441(1)	0.2441(1)	0.2440(1)	0.2443(1)	0.2440(1)
z(H3)	0.447 74(8)	0.448 02(9)	0.447 98(9)	0.448 11(9)	0.448 15(9)	0.448 17(10)	0.448 13(9)	0.448 00(9)
U(H3) (10^{-4} Å^2)	32(3)	38(3)	36(3)	43(3)	47(3)	54(4)	55(3)	64(4)
a	5.652 36(4)	5.652 49(5)	5.652 70(5)	5.652 99(5)	5.653 34(5)	5.653 81(5)	5.654 32(5)	5.655 11(5)
U(Ge) (10^{-4} Å^2)	13(1)	16(1)	18(1)	19(1)	22(1)	25(1)	28(1)	32(1)

165	180	195	210	225	240	260	280	300
6795	6795	6795	6795	6795	6795	6795	6795	6795
4991	4996	5002	5006	5084	5009	5009	5009	5095
66	66	66	66	66	66	65	65	65
3.36	3.42	3.48	3.56	3.37	3.55	3.51	3.44	3.52
4.81	4.83	4.81	4.97	4.66	4.96	4.86	4.85	4.84
5.37	5.31	5.41	5.67	5.13	5.35	5.58	5.52	5.64
4.49	4.52	4.53	5.14	5.14	4.84	5.39	5.18	5.64
4.127 65(6)	4.128 52(6)	4.129 54(6)	4.130 26(6)	4.131 04(6)	4.131 37(6)	4.133 03(5)	4.134 22(5)	4.135 10(5)
11.2610(2)	11.2629(2)	11.2650(2)	11.2668(2)	11.2686(2)	11.2692(2)	11.2735(2)	11.2753(2)	11.2774(2)
13.2113(2)	13.2136(2)	13.2160(2)	13.2180(2)	13.2201(2)	13.2209(2)	13.2257(2)	13.2279(2)	13.2297(2)
0.207 68(8)	0.207 70(8)	0.207 69(8)	0.207 72(8)	0.207 70(8)	0.207 73(8)	0.207 77(8)	0.208 02(8)	0.208 26(8)
72(5)	86(5)	83(5)	108(6)	112(6)	108(6)	107(6)	129(6)	128(6)
106(6)	115(6)	129(6)	139(6)	134(6)	141(6)	165(7)	163(7)	190(7)
180(6)	184(6)	195(6)	206(6)	215(6)	234(6)	268(7)	257(7)	282(7)
−0.0698(1)	−0.0697(1)	−0.0696(1)	−0.0695(1)	−0.0695(1)	−0.0698(1)	−0.0696(1)	−0.0694(1)	−0.0695(1)
0.3437(1)	0.343 79(9)	0.3439(1)	0.3439(1)	0.3437(1)	0.3435(1)	0.3435(1)	0.3437(1)	0.3438(1)
59(3)	61(4)	67(4)	72(4)	71(4)	77(4)	77(4)	76(4)	79(4)
0.0264(1)	0.0264(1)	0.0264(1)	0.0262(1)	0.0264(1)	0.0263(1)	0.0266(1)	0.0267(1)	0.0267(1)
0.4086(1)	0.4089(1)	0.4084(1)	0.4082(1)	0.4083(1)	0.4083(1)	0.4083(1)	0.4085(1)	0.4085(1)
43(3)	52(4)	58(4)	60(4)	63(4)	67(4)	69(4)	75(4)	78(4)
0.2436(1)	0.2439(1)	0.2439(1)	0.2440(1)	0.2440(1)	0.2441(1)	0.2439(1)	0.2044(1)	0.2438(1)
0.447 87(9)	0.447 99(9)	0.448 07(9)	0.4482(1)	0.448 37(9)	0.4481(1)	0.4481(1)	0.4481(1)	0.4479(1)
69(4)	80(4)	82(4)	86(4)	88(4)	89(4)	99(4)	102(4)	107(4)
5.656 36(5)	5.656 97(5)	5.657 72(5)	5.658 30(6)	5.658 77(6)	5.658 83(7)	5.660 46(5)	5.661 12(5)	5.661 68(5)
35(1)	38(1)	43(1)	47(1)	50(1)	52(2)	60(2)	63(2)	66(2)

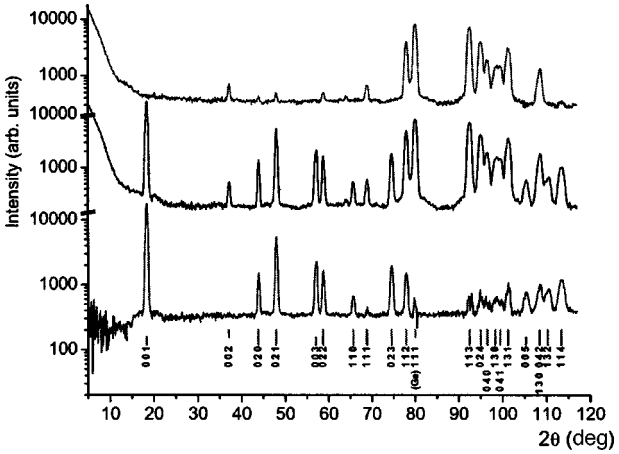

FIG. 2. Neutron powder-diffraction patterns measured with long wavelength at the DMC. The upper curve is above phase-transition temperature at 15 K, the curve in the middle is below the phase-transition temperature at 1.5 K, and the lower curve is the difference between the 1.5- and the 15-K data. The reflection indices are shown at the bottom. The plot is on a logarithmic scale to enhance subtle features, and the curves have been shifted for clarity.

within the chains order ferromagnetically, whereas the magnetic moment of the nearest- and next-nearest-neighbor chains order antiferromagnetically. Even though the ordering of the magnetic moments is one dimensional, the magnetic exchange interaction is three dimensional as indicated in part by the sharp lambda-shaped heat-capacity anomaly at the phase transition.[17] The minimum Eu-Eu distance is the intrachain distance of 4.12 Å. The Eu atoms in the nearest-neighbor chains are at distances of 5.99 Å and the Eu in the next-nearest-neighbor chains are at distances of 6.98 Å (Fig. 3).

The minimum Eu-Eu separation in the ferromagnet EuO (NaCl structure) is 3.64 Å. An explanation for exchange interaction in EuO was proposed by G. ter Maten *et al.*[24] It follows the principles of superexchange seen in MnO, where the magnetization is mediated via the oxygen atom. This kind of exchange is unlikely in the case of clathrates, because the distance to the framework atoms (3.37 Å) is large compared with the distance in the oxide (2.57 Å). The interchain distance in $Eu_4Ga_8Ge_{16}$ is short compared with distances in other Eu-containing clathrates. Kasuya alternatively proposed that the exchange in EuO takes place through a virtual transfer of magnetic $4f$ electrons to the vacant $5d$ orbital, extending to the neighboring $4f$ orbital.[25] The electrons then couple ferromagnetically via *d-f* interaction. The exchange proposed by Kasuya can account for the interchain magnetic order, but not for the antiferromagnetic ordering of the chains in $Eu_4Ga_8Ge_{16}$. The alternating exchange interaction between intrachain and interchain atoms may be explained by the Ruderman-Kittel-Kasuya-Yosida (RKKY) exchange.[26] The RKKY exchange has been suggested to be responsible for the ordering in the ferromagnetic clathrates β-$Eu_8Ga_{16}Ge_{30}$ (5.23 Å) and α-$Eu_8Ga_{16}Ge_{30}$ (5.56 Å),[14] where the distances are between those observed for $Eu_4Ga_8Ge_{16}$. Assuming the RKKY exchange is responsible for the ordering in $Eu_4Ga_8Ge_{16}$, it may be possible to change (or even suppress) the magnetic ordering by controlling the exact framework stoichiometry, i.e., by affecting the charge-carrier concentration. Our sample is a *p*-type conductor,[12] whereas Paschen *et al.* have reported *n*-type conductivity, with an antiferromagnetic ordering temperature at 9 K.[16] However, it must be kept in mind that the material of course is not a free-electron gas and significant deviations from the RKKY model are probable. The size of the exchange interaction is proportional to the electron scattering length, i.e., the exact composition of the sample and the framework disorder. This could explain differences in transitions temperatures among different samples. Note, however, that it is difficult to rule out small systematic errors in temperature recording, when comparing different studies on $Eu_4Ga_8Ge_{16}$ carried out with different instruments.

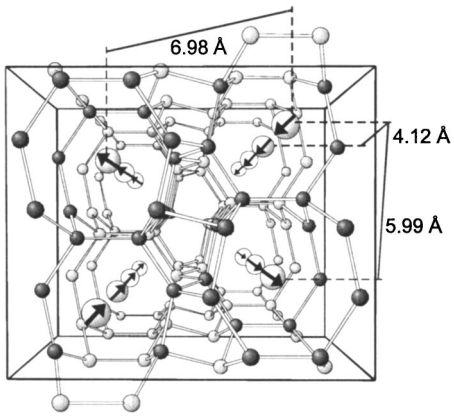

FIG. 3. The magnetic structure of $Eu_4Ga_8Ge_{16}$. The unit-cell content has been depicted with large europium atoms and smaller framework atoms. The perspective is along the *a* axis with the *b-c* axis in the plane of the paper. The Eu-Eu distances are shown.

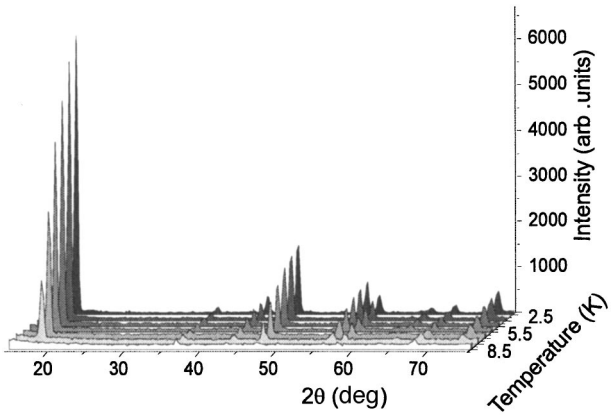

FIG. 4. Neutron powder-diffraction patterns as a function of temperature.

B. Temperature dependence of the magnetic structure

As described in Sec. II A, diffraction data around the phase-transition temperature were measured at the DMC neutron powder diffractometer in the range 1.5–30 K with decreased temperature steps close to the phase transition and at the lowest temperatures. These diffraction patterns are

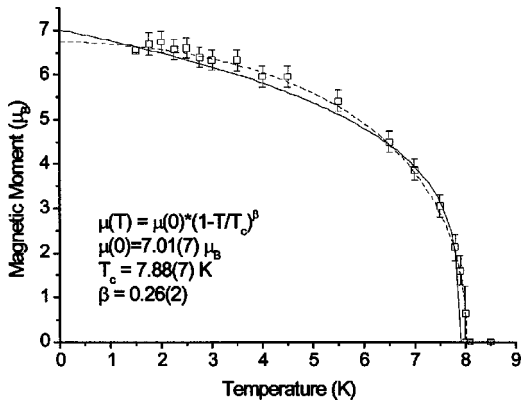

FIG. 5. The refined *a*-axis magnetic moment as a function of temperature. The solid curve is a fit to the power law described in the text. The dashed curve is a guide to the eye.

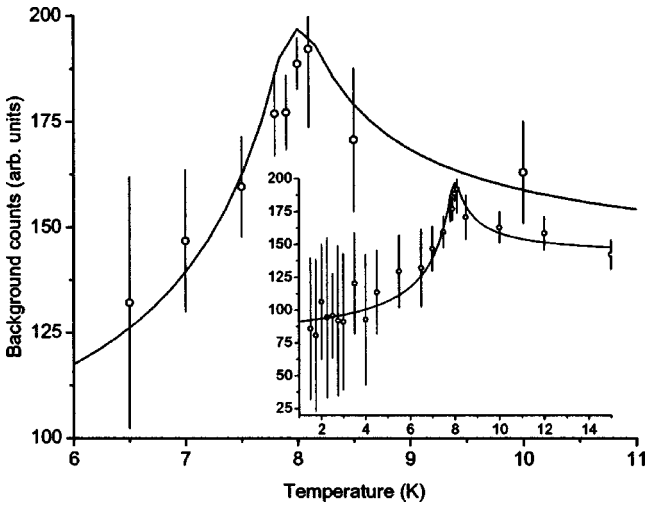

FIG. 6. The temperature dependence of the background scattering below the magnetic 001 peak ($2\theta = 18.4°$) showing a cusp close to T_N. The inset shows the entire data range, and the solid curve serves as a guide to the eye.

shown between 1.5 and 8.5 K in Fig. 4. The plot shows how the magnetic Bragg peaks increase in the diffraction pattern with decreasing temperature. All the diffraction patterns shown in Fig. 4 are obtained for fixed monitor count but with considerably less statistics than in the 1.5- and 15-K data used for the refinement of the magnetic structure discussed in Sec. III A. For the refinement of the 1.5-K data with less statistics all the structural parameters were fixed to the values found from the refinement of the 1.5-K data with good statistics, and only the scale factor, the background, and the zero point were refined. The scale factor obtained from this fit was then used as a common scale factor in the subsequent refinements of the higher temperature data, where the backgrounds, zero-point shifts and the magnetic moments were the only variable parameters.

The unit-cell parameters were refined at each temperature, but no systematic change was observed within the precision of the data. Figure 5 shows the resulting temperature dependence of the *a*-axis magnetic moment from refinement of the multitemperature data. The temperature dependence of the magnetic moments was fitted to the expression $\mu(T) = \mu(0\ \mathrm{K})(1-T/T_N)^\beta$. The magnetic moment at 0 K is found to be $\mu(0\ \mathrm{K}) = 7.01(7)\mu_B$ in agreement with the magnetic moment of the free Eu^{2+} ion. A simple extrapolation of the experimental data to 0 K leads to the slightly lower value of $\sim 6.75\mu_B$. The critical temperature $T_N = 7.88(7)$ K is in accordance with the phase-transition temperature observed by other methods, and the critical exponent is $\beta = 0.26(2)$. The data were also refined with a model having the magnetic moment components along the *a* and *c* axes (not shown). For this model the fit to the power law gave: $\mu(0\ \mathrm{K}) = 6.9(1)\mu_B$, $T_N = 7.8(1)$ K, and $\beta = 0.24(3)$, i.e., statistically identical values.

It is also possible to observe the phase transition in the background below the magnetic peaks. In Fig. 6, the temperature dependence of the diffuse scattering below the 001 Bragg peak ($2\theta = 18.4°$) close to the Néel temperature is shown. As T_N is approached from above, the diffuse scattering of the magnetic moments increases due to short-range order of the magnetic moments and a divergence is observed at the transition temperature. Below T_N the long-range order becomes dominant and gradually the diffuse scattering disappears.

C. Temperature dependence of the crystal structure

In the past few years many studies have focused on the thermal conductivity in open framework structures with the specific aim of understanding the role of the loosely bound guest atoms for the thermal properties.[27,28] In a series of papers Sales and co-workers have shown that a basic crystallographic parameter, the isotropic mean-square displacement parameter U_{iso}, can provide very useful information on the thermal conductivity of crystalline materials.[28] In this description the vibrations of the framework atoms are approximated by the Debye model, while the vibrations of the guest atoms are approximated with the Einstein model. Following Bentien *et al.*[7] and Bürgi and co-workers,[29,30] the Eu atomic displacement factors (ADP's) can be written as

$$\langle U^2 \rangle = d^2 + \frac{\hbar^2}{2mk_B\Theta_E}\coth\frac{\Theta_E}{2T}, \tag{1}$$

where a temperature-independent disorder parameter *d* has been introduced into the normal Einstein oscillator expression. In Fig. 7 the Einstein equation is fitted to the refined Eu ADP's. The plot also shows the ADP's of the framework and of the Ge impurity. These can be fitted to a Debye model:

$$\langle U^2 \rangle = d^2 + \frac{3\hbar^2 T}{mk_B\Theta_D^2}\left(\Phi(\Theta_D/T) + \frac{1}{4}\cdot\frac{\Theta_D}{T}\right). \tag{2}$$

For the framework atoms of $Eu_4Ga_8Ge_{16}$ the mass weighted average value for the three different sites is used. The results of the fits are shown in Table III. For the Eu guest atom there is a clear disorder along the *c* axis. This suggests that Eu atoms are not placed in the centers of the cages although the present data do not allow discrimination between a very shal-

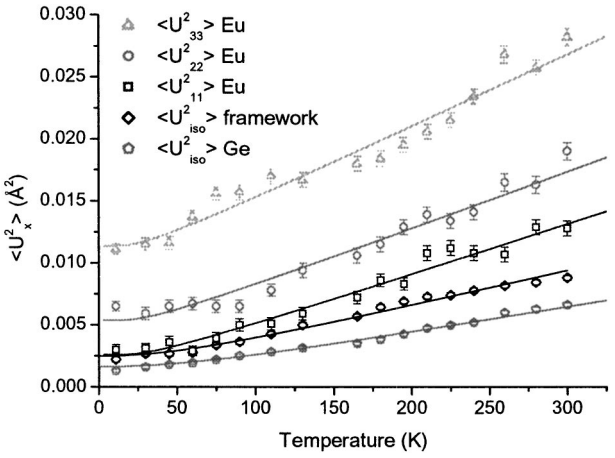

FIG. 7. The ADP's along the different axes for Eu, the isotropic ADP's for the framework atoms (Ge/Ga), and the ADP's for the Ge impurity. The framework and the impurity (Ge) ADP's have been fitted to a Debye model, and the Eu ADP's to an Einstein model.

low potential with a minimum in the center and one with a (small) maximum at the average Eu position. The Eu disorder gives a plausible explanation for why the modeling of the magnetic moments gave a component along the *c* axis in an unconstrained model. It should be noted that the choice of model for the Eu guest atom is somewhat arbitrary. An equally good fit of the Eu ADP's can be obtained if a Debye model is used. Nevertheless, use of an Einstein model yields an Einstein temperature, which is excellent agreement with values obtained from modeling of completely different physical quantities (heat capacity and Mossbauer data), and this supports that the guest atoms to a first approximation can be considered as independent oscillators. From the ADP modeling of the framework atoms we obtain a Debye temperature of 266(4) K for the $Eu_4Ga_8Ge_{16}$ phase and 311(4) K for the Ge impurity phase. The value for Ge is somewhat lower than one value of 360 K reported in the literature.[31] The thermal expansion has also been extracted from the Rietveld refinement results and discussed elsewhere.[32]

In Paper II the measured heat capacity of $Eu_4Ga_8Ge_{16}$ was fitted to a Debye model giving $\Theta_D = 314(4)$.[17] It may be argued that accurate single-crystal data normally will give more reliable estimates of ADP's than powder data. However, the present synchrotron powder diffraction data have the advantage that no extinction or absorption corrections are needed. These corrections can significantly influence the ADP's. Furthermore, in the present case we use a fit to 15 independent data sets with the full Debye model rather than a simple room-temperature approximation to one data point. Our data also have a very high resolution in reciprocal space, which facilitates accurate modeling of the ADP's. Heat-capacity measurements are ''contaminated'' by small contributions from the electrons and significantly larger contributions from the magnetic heat capacity. These contributions must be subtracted from the measured data assuming several approximations. All in all the value extracted from the multitemperature ADP's probably is the most accurate.

TABLE III. Parameters obtained from Einstein and Debye fits to the ADP's.

	Θ_E (K)	Θ_D (K)	d^2 (Å^2)
$\langle U^{11}\rangle$Eu	88(2)		0.0008(3)
$\langle U^{22}\rangle$Eu	83(2)		0.0034(4)
$\langle U^{33}\rangle$Eu	74(2)		0.0092(5)
$\langle U_{\rm iso}\rangle$Ga/Ge		266(4)	0.0006(2)
$\langle U_{\rm iso}\rangle$Ge (impurity)		311(4)	

From the Debye temperature $[\Theta_D = 266(4)\ \mathrm{K}]$ obtained from the ADP fits we can estimate the lattice contribution to the thermal conductivity.[28] The Debye temperature gives the speed of sound in the solid. The heat capacity was measured at 266 K to be $C_\nu = 1.79\ \mathrm{J/cm^3\,K}$ and the mean free path of the phonons may be approximated by the mean Eu-Eu separation in the unit cell (5.7 Å). The lattice contribution to the thermal conductivity can now be estimated from $\kappa_{\rm Lattice} = \frac{1}{3} V_s d C_\nu$. At 266 K we obtain 0.0125 W/cm K for $Eu_4Ga_8Ge_{16}$, which is in between typical values of skutterudites and type-I clathrates. Since the lattice thermal conductivity is a slowly changing function of temperature, we may also take this value to be valid at room temperature. It is possible to estimate the thermoelectric figure of merit at room temperature, knowing the Seebeck coefficient and electrical conductance, which is 40 μV/K and 130 S/cm, respectively, at room temperature.[12] The electric contribution to the thermal conductivity is estimated from Wiedemann-Franz law $\kappa_e/\sigma T = 2.22\times10^{-8}\ \mathrm{W\,\Omega/K^2}$. This gives a dimensionless figure of merit $ZT = T(S^2\sigma/\kappa)$ equal to 4.6×10^{-3}, which is too low for room-temperature thermoelectric applications.

IV. CONCLUSION

In this study the antiferromagnetic structure of the $Eu_4Ga_8Ge_{16}$ clathrate is established based on neutron powder-diffraction measurements. The magnetic moment was found to have intrachain ferromagnetic order along the *a* axis. Each Eu chain has an interchain antiferromagnetic ordering with the nearest- and next-nearest-neighbor Eu chains. Modeling the temperature dependence of the ordered magnetic moment to a power law results in a 0-K magnetic moment value of $7.01(7)\mu_B$, which is in agreement with the value for the free Eu^{2+} ion. From multitemperature synchrotron powder-diffraction data structural parameters were determined by the Rietveld method. Analysis of the Eu ADP's gave evidence for structural disorder along the *c* axis on the guest atom sites. Modelling of the framework ADP's with a Debye model provided an estimate of the Debye temperature of 266(4) K. This subsequently gives a lattice contribution to the thermal conductivity of 0.0125 W/cm K and a room-temperature thermoelectric figure of merit of 4.6×10^{-3}.

ACKNOWLEDGMENTS

We gratefully acknowledge the assistance during the measurements of Dr. L. Keller, Dr. P. Fischer, and Dr. Eiji Nishibori. We also thank the Paul Scherrer Institute and The Japa-

nese Synchrotron Radiation Facility (SPring8) for beam time. The work was supported in part by the DANSYNC Center under the Danish Research Councils and by the office of Naval Research (Contract No. N00014-99-1-0266). H.B. thanks the Danish Natural Sciences Research Council for additional support.

*Corresponding author. Electronic address: bo@chem.au.dk

[1] G. S. Nolas, J. L. Cohn, G. A. Slack, and S. B. Schjuman, Appl. Phys. Lett. **73**, 178 (1998).
[2] J. L. Cohn, G. S. Nolas, V. Fessatidis, T. H. Metcalf, and G. A. Slack, Phys. Rev. Lett. **82**, 779 (1999).
[3] V. L. Kuznetsov, L. A. Kuznetsova, A. E. Kaliazin, and D. M. Rowe, J. Appl. Phys. **87**, 7871 (2000).
[4] A. Bentien, A. E. C. Palmqvist, J. D. Bryan, S. Latturner, G. D. Stucky, L. Furenlid, and B. B. Iversen, Angew. Chem., Int. Ed. Engl. **40**, 1262 (2000).
[5] B. B. Iversen, A. E. C. Palmqvist, D. E. Cox, G. S. Nolas, G. D. Stucky, N. P. Blake, and H. Metiu, Solid State Commun. **149**, 455 (2000).
[6] B. C. Chakoumakos, B. C. Sales, D. Mandrus, and G. S. Nolas, J. Alloys Compd. **296**, 80 (2000).
[7] A. Bentien, B. B. Iversen, J. D. Bryan, G. D. Stucky, A. E. C. Palmqvist, A. J. Schultz, and W. J. Henning, J. Appl. Phys. **91**, 5694 (2002).
[8] J. D. Bryan, N. P. Blake, H. Metiu, G. D. Stucky, B. B. Iversen, R. D. Poulsen, and A. Bentien, J. Appl. Phys. **91**, 7281 (2002).
[9] Y. Mudryk, P. Rogl, C. Paul, S. Berger, E. Bauer, G. Hilscher, C. Godart, and H. Noël, J. Phys.: Condens. Matter **14**, 7991 (2002).
[10] S. Bobev and S. C. Sevov, J. Solid State Chem. **153**, 92 (2000).
[11] S. Latturner, B. B. Iversen, J. Sepa, V. Srdanov, and G. D. Stucky, Phys. Rev. B **63**, 125403 (2001).
[12] J. D. Bryan and G. D. Stucky, Chem. Mater. **13**, 253 (2001).
[13] W. Carrillo-Cabrera, S. Paschen, and Y. Grin, J. Alloys Compd. **333**, 4 (2002).
[14] B. C. Chakoumakos, B. C. Sales, and D. G. Mandrus, J. Alloys Compd. **322**, 127 (2001).
[15] B. C. Sales, B. C. Chakoumakos, R. Jin, J. R. Thompson, and D. Mandrus, Phys. Rev. B **63**, 245113 (2001).
[16] S. Paschen, W. Carrillo-Cabrera, A. Bentien, V. H. Tran, M. Baenitz, Yu. Grin, and F. Steglich, Phys. Rev. B **64**, 214404 (2001).
[17] J. D. Bryan, H. Trill, H. Birkedal, M. Christensen, V. I. Srdanov, H. Eckert, B. B. Iversen, and G. D. Stucky, following paper, Phys. Rev. B **68**, 174429 (2003).
[18] J. D. Bryan, Ph.D. thesis, Department of Chemistry and Biochemistry, University of California, Santa Barbara, 2002.
[19] J. Rodríguez-Carvajal, FULLPROF program, 2001.
[20] E. Nishibori, M. Takata, K. Kato, M. Sakata, Y. Kubota, S. Aoyagi, Y. Kuroiwa, M. Yamakata, and N. Ikeda, Nucl. Instrum. Methods Phys. Res. A **467**, 1045 (2001).
[21] A. C. Larson and R. B. von Dreele, GSAS Program, Los Alamos National Laboratory Report LAUR 86-748, 2000.
[22] A. S. Wills, Physica B **276**, 680 (2000).
[23] A. S. Wills, J. Phys. IV **11**, 133 (2001).
[24] G. ter Maten and L. Jansen, Physica B **95**, 11 (1978).
[25] T. Kasuya, IBM J. Res. Dev. **14**, 214 (1970).
[26] C. Kittel, Solid State Phys. **22**, 1 (1968).
[27] B. C. Sales, D. Mandrus, and B. C. Chakoumakos, Semicond. Semimetals **70**, 1 (2000).
[28] S. B. Schujman, G. S. Nolas, R. A. Young, C. Lind, A. P. Wilkinson, G. A. Slack, R. Patschke, M. G. Kanatzidis, M. Ulutagay, and S. J. Hwu, J. Appl. Phys. **87**, 1529 (2000).
[29] H. B. Bürgi, Annu. Rev. Phys. Chem. **51**, 275 (2000).
[30] H. B. Bürgi and S. C. Capelli, Acta Crystallogr., Sect. A: Found. Crystallogr. **56**, 403 (2000).
[31] N. W. Ashcroft and N. D. Mermin, *Solid State Physics* (Saunders, Philadelphia, 1976).
[32] H. Birkedal, J. D. Bryan, G. D. Stucky, M. Christensen, and B. B. Iversen, in MRS Symposia Proceedings No. 755 (Materials Research Society, Pittsburg, 2003), DD10.2.1–DD10.2.6.